

Article

# Luminescence of Binary-Doped Silica Aerogel Powders: A Two-Step Sol-Gel Approach

Dimitar Shandurkov, Nina Danchova, Tony Spassov , Vesselin Petrov and Stoyan Gutzov \* 

Faculty of Chemistry and Pharmacy, Sofia University St. Kliment Ohridski, 1164 Sofia, Bulgaria; fhds@chem.uni-sofia.bg (D.S.); ndanchova@chem.uni-sofia.bg (N.D.); tpassov@chem.uni-sofia.bg (T.S.)  
\* Correspondence: fhsg@chem.uni-sofia.bg

**Abstract:** In this study, we report a novel synthesis of hydrophobic silica aerogel powder composites, functionalized and binary-doped with  $[\text{Tb}(\text{phen})_2](\text{NO}_3)_3$  and  $[\text{Eu}(\text{phen})_2](\text{NO}_3)_3$  nanocrystals, employing a two-step sol-gel methodology. The investigation delves into the structural elucidation, optical properties and thermal conductivity of these functionalized Tb(III)-Eu(III) composites. Our analysis includes diffuse reflectance spectra and excitation and luminescence spectra, highlighting the quantum yields of composites with varying chemical compositions. Remarkably, these samples exhibit a strong luminescence, with distinct hues of red or green based on the specific doping type and level. The detailed examination of excitation spectra and quantum yields establishes robust energy-transfer mechanisms from the 1,10-phenanthroline molecule to the lanthanide ions. Notably, our study uncovers a  $\text{Tb}^{3+} \rightarrow \text{Eu}^{3+}$  energy-transfer phenomenon within the binary functionalized samples, providing compelling evidence for a structural formation process occurring within the mesoporous framework of the aerogel powders.

**Keywords:** aerogel powders; luminescence; europium; terbium; energy transfer; thermal conductivity



**Citation:** Shandurkov, D.; Danchova, N.; Spassov, T.; Petrov, V.; Gutzov, S. Luminescence of Binary-Doped Silica Aerogel Powders: A Two-Step Sol-Gel Approach. *Gels* **2024**, *10*, 104. <https://doi.org/10.3390/gels10020104>

Academic Editors: Robert Edward Przekop, Bogna Sztorch and Eliza Romanczuk-Ruszk

Received: 20 December 2023  
Revised: 24 January 2024  
Accepted: 25 January 2024  
Published: 27 January 2024



**Copyright:** © 2024 by the authors. Licensee MDPI, Basel, Switzerland. This article is an open access article distributed under the terms and conditions of the Creative Commons Attribution (CC BY) license (<https://creativecommons.org/licenses/by/4.0/>).

## 1. Introduction

Optical composite materials, based on aerogels and doped with functional nanocrystals, are increasingly important in LED technologies, microelectronics and sensorics. Due to their high specific surface area and porosity, silica aerogel matrices have the possibility of incorporating hybrid molecules and d- and f-ions with desired electrical and optical properties [1]. This is the reason for an increasing number of papers dealing with the preparation and characterization of functional aerogel composites and aerogels including their physical properties and physicochemical preparation strategies.

The first known publication that we encountered with optical composites based on silica hydrophobic aerogels shows the possibility of obtaining composites with the composition  $\text{SiO}_2(\text{aerogel}):[\text{Eu}(\text{phen})_2](\text{NO}_3)_3$  using a two-step sol-gel process [2].

In the next contribution, knowledge of this process was extended by finding dependences of the quantum yield (QY) and spectral intensities of  $\text{SiO}_2:[\text{Eu}(\text{phen})_2](\text{NO}_3)_3$  and  $\text{SiO}_2:[\text{Tb}(\text{phen})_2](\text{NO}_3)_3$  composites on the degree of hydrophobicity,  $\alpha$ , of the starting aerogel matrix [3]. In the same paper, an increased thermal stability of these composites, up to 200 °C, is shown, compared to that of hydrophilic sol-gel composites. Thus, the hydrophobization of silicate surfaces affects the quantum yield of the obtained luminescent materials, reducing the concentration of surface OH groups and at the same time increasing the thermal stability of the obtained aerogel granules [4]. Stable green- or red-emitting materials enable the production of LED additives and the production of multi-color-emitting aerogel powders [5].

The aim of the present contribution is to obtain  $\text{SiO}_2(\text{aerogel}):[\text{Eu}(\text{phen})_2](\text{NO}_3)_3$  and  $[\text{Tb}(\text{phen})_2](\text{NO}_3)_3$  binary optical composites using a two-step sol-gel approach and to investigate their optical properties and thermal conductivity as a part of the following framework: the preparation–structure–properties of gel composites. To the best of our knowledge,

there are no contributions dealing with binary hybrid nanocrystallites incorporated into silica aerogels. The spectral properties of the activator compounds  $[\text{Tb}(\text{phen})_2](\text{NO}_3)_3$  and  $[\text{Eu}(\text{phen})_2](\text{NO}_3)_3$  could be an indicator for phase formation, which takes place in the porous network of the aerogel matrixes.

Inorganic silicate materials containing  $\text{Eu}^{3+}$  and  $\text{Tb}^{3+}$  are already known from a number of publications with a theoretical and applied focus [6–11]. Moreover, binary lanthanide aerogels are prepared during the search for porous materials with suitable optical and catalytic activities [12]. The mixed binary and ternary lanthanide oxide phases are also well-known examples of high-entropy materials [13].

## 2. Experimental Results

The UV-Vis-NIR spectra of binary-doped samples and non-hydrophobized and non-functionalized silica powders (notes GR0) are shown in Figure 1. All silica samples display overtones and combinational vibrations attributed to  $\text{SiO}_2$  in the range of 2250–2400 nm. Even the hydrophobic samples have some traces of residual water according to the spectra in the NIR region. Water molecules have two intense overtones in the near-infrared region. The peaks are centered around 1940 and 1450 nm. The luminescent samples also display peaks at 1186 nm and doublets at 1696 and 1745 nm. These bands are associated with combinational and overtone vibrations of C-H groups in aromatic compounds; however, the positions of the maxima are slightly shifted compared to C-H energies in pure benzene. This means they most likely originate from the 1,10-phenanthroline (phen) molecule, and the shift of the maxima is due to the presence of an N-heteroatom in the aromatic ring of the molecule [14].

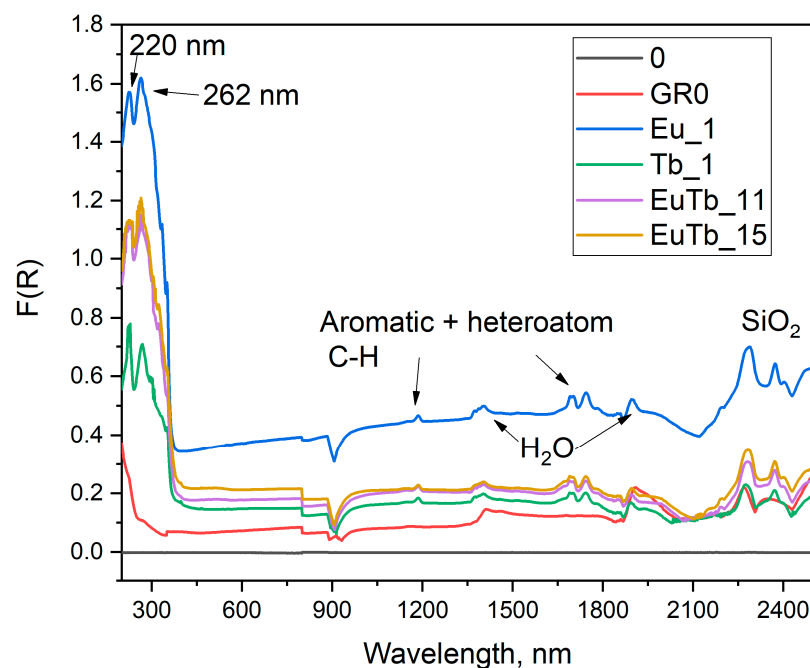


**Figure 1.** UV-Vis-NIR spectra of the samples. Notations: 0—reference; GR0—non-doped  $\text{SiO}_2$  sol-gel sample. The chemistry of the samples is given in Tables 1 and 2. Eu\_Tb denotes binary-doped composites; Eu\_1 and Tb\_1 contain  $\text{Eu}^{3+}$  or  $\text{Tb}^{3+}$  only.

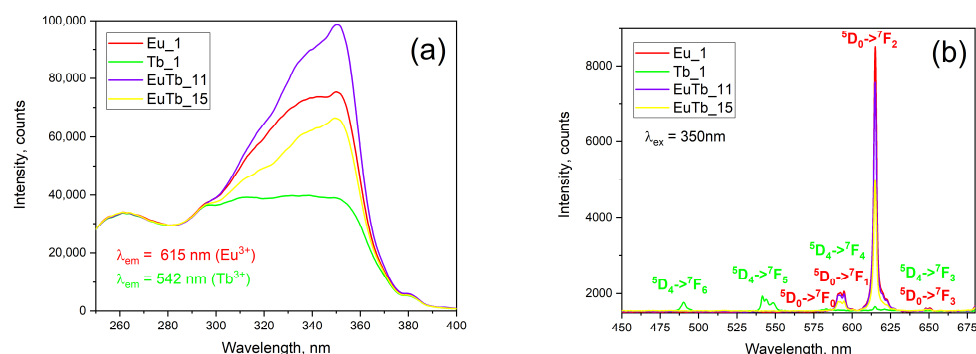
**Table 1.** Thermal properties of the investigated samples at room temperature. The experimental error of the density is about 5%.

Sample	$\alpha$	$\lambda$ W/m.K	$\Delta\lambda$ W/m.K	$W.s^{1/2}/m^2.K$	$W.s^{1/2}/m^2.K$	$\rho$ g/cm <sup>3</sup>	$n_{Ln}/n_{SiO_2}$
GR0	0	0.0640	0.0002	145.3896	0.8531	0.45	0
Eu_1	1.1	0.0523	0.0001	95.6041	0.5516	0.23	0.01
Tb_1	1.1	0.0467	0.0001	71.2591	0.5505	0.18	0.01
EuTb_11	1.1	0.0510	0.0001	90.2086	0.4896	0.18	0.01
EuTb_15	1.1	0.0523	0.0003	95.5750	1.1232	0.18	0.01

**Table 2.** Summary of the optical properties of the composite samples: sample name, chemical composition, quantum yield, relative intensity ratio and CIE-1931 color coordinates of the emission.

Sample	Chemistry	QY, Red %	QY, Green %	$I_{ED}/I_{MD}$	x	y	z
GR0	SiO <sub>2</sub>	-	-	-	-	-	-
Tb_1	SiO <sub>2</sub> :0.01Tb	-	6.3	0.39	0.631	0.340	0.03
Eu_1	SiO <sub>2</sub> :0.01Eu	35	-	5.98	0.358	0.486	0.156
EuTb1_1	SiO <sub>2</sub> :0.005Eu;0.005Tb	30	-	5.92	0.626	0.336	0.038
EuTb1_5	SiO <sub>2</sub> :0.0017Eu;0.0083Tb	32	-	6.06	0.597	0.322	0.081
Euphen	[Eu(phen) <sub>2</sub> ](NO <sub>3</sub> ) <sub>3</sub> [2,3]	35	-	7.25	0.309	0.602	0.089
Tbphen	[Tb(phen) <sub>2</sub> ](NO <sub>3</sub> ) <sub>3</sub> [2,3]	-	13	0.37	0.665	0.333	0.003

Figure 2a,b shows the excitation and emission spectra, respectively, of the composite samples. The excitation spectra do not follow the reflectance spectra.

**Figure 2.** (a) Excitation spectra of the luminescent composite sample; (b) Emission spectra of the samples. Electronic f-f transitions are given: green for Tb<sup>3+</sup> and red for Eu<sup>3+</sup> ions. The chemistry of the samples is given in Tables 1 and 2. Eu\_Tb denotes binary-doped composites; Eu\_1 and Tb\_1 contain Eu<sup>3+</sup> or Tb<sup>3+</sup> only.

The thermal properties of the composites are summarized in Table 1. The table contains the degree of hydrophobicity ( $\alpha$ ), the thermal conductivity ( $\lambda$ ), the effusivity ( $e$ ), and the bulk density ( $\rho$ ) of the samples.

The aerogel-like character of the functionalized composites investigated here is demonstrated by their low thermal conductivities, which comes from their high porosity. Such an observation proves the effectivity of the aerogel powder drying conditions applied for hydrophilic and hydrophobic species. The thermal properties of low-doped, hydrophobic aerogel powders with the composition SiO<sub>2</sub>:[Ln(phen)<sub>2</sub>](NO<sub>3</sub>)<sub>3</sub> and  $n_{Ln}/n_{SiO_2} = 0.0035$  and  $\alpha = 1.1$  [3] are very close to that of highly doped composites:  $\lambda = 0.048$  W/m.K,  $e = 76$  W.s<sup>1/2</sup>/m<sup>2</sup>.K, and a density of 0.18 g/cm<sup>3</sup>.

The thermal conductivity and effusivity of the pure, powdered dopants—[Tb(phen)<sub>2</sub>](NO<sub>3</sub>)<sub>3</sub> and [Eu(phen)<sub>2</sub>](NO<sub>3</sub>)<sub>3</sub>—are 0.057 W/m<sup>2</sup>.K and 0.059 W/m.K and 116.5 W.s<sup>1/2</sup>/m<sup>2</sup>.K and 125.2 W.s<sup>1/2</sup>/m<sup>2</sup>.K, respectively.

X-ray diffraction measurements prove that the optically active nanocrystallites in this study display a structural polymorphism (Figure 3). The  $[\text{Eu}(\text{phen})_2](\text{NO}_3)_3$  and  $[\text{Tb}(\text{phen})_2](\text{NO}_3)_3$  are isostructural, with small differences in the cell parameters. However,  $[\text{Eu}(\text{phen})_2](\text{NO}_3)_3$  has two polymorphs, formed depending on the reaction conditions [14]. Lindenberg et al. [14] provide the following cell parameters for the second  $[\text{Eu}(\text{phen})_2](\text{NO}_3)_3$  phase:  $a = 9.515$ ,  $b = 15.454$ ,  $c = 17.176$  Å, and  $\beta = 93.45^\circ$  with a space group of  $P2_1/c$ . The pure powdered  $[\text{Eu}(\text{phen})_2](\text{NO}_3)_3$  complex crystallizes in a monoclinic phase, as described by Mirochnik et al. [15]. The XRD pattern of this phase is shown in Figure 3 as Euphen\_th (black line), while the theoretical patterns of the  $[\text{Tb}(\text{phen})_2](\text{NO}_3)_3$  are given as Tbphen\_th (green line). The PowderCell program [16] was applied to construct the XRD pattern using data collected from the crystal structure information. The crystals are monoclinic, with the space group  $C2/c$ . The cell parameters are  $a = 11.168(1)$ ,  $b = 17.976(2)$ ,  $c = 13.053(1)$  Å, and  $\beta = 100.577(2)^\circ$ . The XRD pattern for the  $\text{Tb}^{3+}$  complex was constructed using structure data from the literature [17]. Hence, being isostructural, the two complexes display very similar XRD patterns.

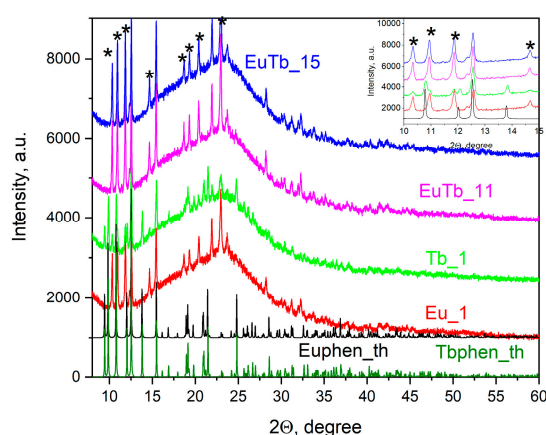


**Figure 3.** XRD patterns of the binary composite samples. The peaks originating from the second  $[\text{Eu}(\text{phen})_2](\text{NO}_3)_3$  phase are marked with \*. The notations Euphen\_th and Tbphen\_th refer to theoretical X-ray diffraction patterns of the pure crystalline components:  $[\text{Eu}(\text{phen})_2](\text{NO}_3)_3$  and  $[\text{Tb}(\text{phen})_2](\text{NO}_3)_3$ .

In agreement with the above-mentioned results, the X-ray diffraction patterns here show the presence of both structures, and the peaks of the phase observed by Lindenberg et al. [14] are marked with \*. Thus, we can conclude that a mixture of the two polymorphic forms of  $[\text{Ln}(\text{phen})_2](\text{NO}_3)_3$  is obtained in the pores of the silica gels during the in-situ preparation procedure. The mean crystallite size of the crystallites obtained by the X-ray diffraction analysis is about 20 nm.

No diffraction patterns originating from  $\text{Eu}(\text{NO}_3)_3$ ,  $\text{Tb}(\text{NO}_3)_3$ , or solid 1,10-phenanthroline and their possible crystal hydrates were detected. It should also be stressed that the interpretation of the XRD pattern of the samples is hampered by the low concentration of the dopant (1%) and the presence of an intense, broad amorphous halo originating from the silica matrix [4]. Therefore, the formation of a new nanostructure in the pores of the silica matrix with the composition  $[\text{Eu},\text{Tb}(\text{phen})_2](\text{NO}_3)_3$  cannot be excluded.

### 3. Discussion

#### 3.1. Optical Properties

Due to the low concentration of the  $\text{Ln}^{3+}$  (1%) complex in the matrix, the f-f transition in the ions is not visible in the reflection spectra of the samples (Figure 1). These transitions are forbidden by the Laporte selection rules and have a low oscillator strength, and, therefore, a low intensity. The UV region of the reflectance spectra is dominated by ligand (phen) and matrix ( $\text{SiO}_2$ ) absorption bands. The 1,10-phenanthroline molecule has a strong and broad absorption band around 350 nm, which is seen as a shoulder in the reflectance spectra. This

is the most important excitation channel in these complexes and the composite materials doped with them. The energy is transferred through the following path: first, the UV photon (350 nm) is absorbed by the 1,10-phenanthroline molecule and it is excited to the first singlet state. Afterward, the 1,10-phenanthroline molecule relaxes non-radiatively to its first triplet state. There onwards, through the process of intersystem crossing, the ligand molecule transfers the energy to the emitting level of the lanthanide ion. A simplified energy-transfer scheme is  $S_0 \rightarrow S_1 \rightarrow T_1 \rightarrow {}^5D_J(\text{Ln}^{3+})$  [3,18]. Furthermore, very intense ligand-to-metal charge transfer transitions (CTTs) are visible in the UV region at around 220 nm and 260 nm. It is well-known that an  $O^{2-} \rightarrow \text{Ln}^{3+}$  transition is observed in oxide matrices [6,19,20]. These transitions partially overlap with some 1,10-phenanthroline peaks in the UV region (232 and 265 nm).

The excitation spectra in this work clearly show three distinct energy-transfer pathways in the luminescent  $[\text{Ln}(\text{phen})_2](\text{NO}_3)_3$  complexes, depending on the dopant type and doping level. The first is the ligand-to-metal  $O^{2-} \rightarrow \text{Ln}^{3+}$  CTT at 260 nm. The second and the most intense is the ligand-to-metal resonant energy transfer described above. This transition occurs when the ligand is excited with UV light with a wavelength of around 350 nm. Similar to our previous findings, this energy transfer from 1,10-phenanthroline molecules is more efficient for the  $\text{Eu}^{3+}$  complex rather than for the  $\text{Tb}^{3+}$  one [3]. The resonant energy transfer in hybrid molecules is the most efficient when the triplet  $T_1$  state of the ligand is 2000–3000  $\text{cm}^{-1}$  above the metal receiving level ( ${}^5D_J$ ,  $J = 0, 1, 2$  for  $\text{Eu}^{3+}$  and  $J = 3, 4$  for  $\text{Tb}^{3+}$ ) [6]. This ensures there is little-to-no back energy transfer from the metal ion to the ligand molecule. The last energy-transfer path is via the direct excitation of the lanthanide ion (380–390 nm). This is the least-efficient excitation path due to the forbidden nature of the f-f transition. The intensity of this transition is about 1/10th of the intensity of the FRET transition visible at about 350 nm.

Luminescent materials doped with  $\text{Tb}^{3+}$  or  $\text{Eu}^{3+}$  ions are well known for their excellent light-emission properties in the green or red spectral region, which are responsible for many applications such as tricolor luminescent lamps, LED components, and sensors [19].

The emission spectra, shown in Figure 2b, display the well-known f-f transition peaks for the  $\text{Eu}^{3+}$  and  $\text{Tb}^{3+}$  emission. The mixed samples, containing  $\text{Eu}^{3+}$  and  $\text{Tb}^{3+}$ , do not show any detectable emission originating from  $\text{Tb}^{3+}$  ions. This effect is discussed in the following paragraphs. Samples Eu\_1, EuTb\_11 and EuTb\_15 have only  $\text{Eu}^{3+}$  emission peaks. We can observe  ${}^5D_0-{}^7F_J$  ( $J = 1, 2, 3$ ) transitions. The most intense is the f-f electric dipole transition  ${}^5D_0-{}^7F_2$  at 615 nm, which gives the distinct red emission color of the  $\text{Eu}^{3+}$ -doped composites. The only sample exhibiting green  $\text{Tb}^{3+}$  emission is the one doped with the pure  $[\text{Tb}(\text{phen})_2](\text{NO}_3)_3$  complex, namely sample Tb\_1. In Figure 2b, one can observe the  ${}^5D_4-{}^7F_J$  ( $J = 6, 5, 4, 3, 2$ ) transitions. The most intense  $\text{Tb}^{3+}$  peak is the  ${}^5D_4-{}^7F_5$  transition, centered at 542 nm, giving the green color of the emission.

The optical properties of the aerogel nanocomposites are summarized in Table 1. The relative spectral intensities between the electro-dipole and magnetic-dipole transitions clearly indicate a low site symmetry, of  $C_{2V}$  or lower, around the  $\text{Ln}^{3+}$  ions [19,21]. For the  $[\text{Eu}(\text{phen})_2](\text{NO}_3)_3$  complex, the ratio between the electro-dipole transition  ${}^5D_0-{}^7F_2$  and the magnetic-dipole transition  ${}^7D_0-{}^7F_1$  is calculated. The calculated ratios for samples Eu\_1, EuTb\_11 and EuTb\_15 are 5.98, 5.92 and 6.06, respectively; they are lower than the calculated ratio for the pure  $[\text{Eu}(\text{phen})_2](\text{NO}_3)_3$  complex. This indicates some structural changes and inhomogeneity forming during the in-situ formation of the nanocrystallites inside the silica gel pores. The intensity ratios for the composites are similar in value but they tend to increase when a higher concentration of  $\text{Tb}^{3+}$  is used. This indicates a lowering of the site symmetry around  $\text{Eu}^{3+}$  ions or an increased polarizability of the phen ligand in the different environments [19].

The  $\text{Tb}^{3+}$  ion's f-f electron transitions are less site-sensitive than the electro-dipole transition  ${}^5D_0-{}^7F_2$  in the  $\text{Eu}^{3+}$  ion. For this reason,  $\text{Tb}^{3+}$  is rarely used as a spectroscopic probe. Nevertheless, different relative intensities in the emission peaks of the  $\text{Tb}^{3+}$  ion still indicate some structural and site changes around the ion. There is no definitive procedure to

determine the site symmetry around the  $Tb^{3+}$  ion from the emission spectra, although there is one developed for  $Eu^{3+}$ . The intensity ratio  ${}^5D_4\text{-}{}^7F_6$  to  ${}^5D_4\text{-}{}^7F_5$  is calculated for sample Tb\_1: its value is 0.39 and is close to the ratio for the pure complex  $[Tb(phen)_2](NO_3)_3$ —37 [6,22].

In Table 2, quantum yield, spectral ratio and CIE-1931 color coordinates are compared to that of the pure solid complexes. It is visible that the  $Tb^{3+}$  green f-f emission is suppressed by the  $Eu^{3+}$  doping, which indicates a possible energy transfer of 1,10-phenanthroline  $\rightarrow Tb^{3+} \rightarrow Eu^{3+}$ . Such an assumption correlates with the Diecke diagrams of the terbium and europium ions. The energy of the emitting  $Tb^{3+}$  level  ${}^5D_4$  ( $20,660\text{ cm}^{-1}$ ) is slightly above the two lowest energy levels of  $Eu^{3+}$  ion ( ${}^5D_0$  and  ${}^5D_1$  with energy  $17,240$  and  $21,550\text{ cm}^{-1}$ , respectively). The next energy level of  $Tb^{3+}$   ${}^5D_3$  ( $26,315\text{ cm}^{-1}$ ) has a similar energy to  $Eu^{3+}$   ${}^5G_8$  and is above  ${}^5L_6$  ( $25,450\text{ cm}^{-1}$ ) and  ${}^5D_3$  ( $24,100\text{ cm}^{-1}$ ) [23–25]. Binnenmans et al. [6,19] predict such behavior. The relative spectral intensities are expressed through the ratio  $I_{ED}/I_{MD}$ , which is a semi-quantitative indicator for the site symmetry of the lanthanide ions [20]. The assumption of a  $Tb^{3+} \rightarrow Eu^{3+}$  transfer is supported by the relative peak intensities in the excitation spectra (Figure 2a) at 350 nm.

According to the concept of Foerster resonant energy transfer (FRET), the intensity of the transfer is inversely proportional to the distance between the species. The mean distance between the europium and terbium ions, incorporated into the pores of the aerogels, is less than 10 nm. Such an assumption is well supported by texture investigations of the silica matrix, showing a mean pore diameter of about 7 nm [4]. The in-situ formation of a binary  $[Eu\text{-}Tb(phen)_2](NO_3)_3$  nanostructure in the pore system during the two-step activation requires additional structure investigations, which will be a subject of the next contribution.

The quantum yield (QY) of the samples containing  $Eu^{3+}$  is similar to that of the pure powder complex  $[Eu(phen)_2](NO_3)_3$ . The QY of the samples with europium is 30–35%, and that of the pure complex is 35%. Sample Tb\_1 has a QY of 6.3%, which is half the QY of the pure  $Tb^{3+}$  complex (13%). This could be due to concentration quenching or strong non-radiative relaxation. Glasses and ceramics doped with europium usually display significant concentration quenching above 5% dopant [26]. Both the intensity ratio and CIE-1931 color coordinates suggest structural changes in the optical active species, connected with the binary doping.

### 3.2. Structure and Thermal Conductivity

It is shown that hydrophobization with trimethylchlorosilane (TMCS) leads to a decrease in thermal conductivity by about 20%, which is not dependent on the kind of dopant. It is also known that hydrophobization of the silica matrix also leads to an increase in the mean pore diameter [4]. The values of the thermal conductivity and effusivity obtained are in good agreement with the thermal conductivity vs. density dependence of porous silicate materials [16,27]. Since the thermal conductivity and effusivity of the pure crystalline dopants are very close to that of the matrix and do not affect significantly the composite properties, it can be concluded that the thermal properties of the composites are limited by the degree of hydrophobization and the pore architecture. The doping level also does not affect significantly the thermal properties of the samples.

The polymorphism observed in the present study (Figure 3) and the small size of the crystallites of  $[Eu(phen)_2](NO_3)_3$  and  $[Tb(phen)_2](NO_3)_3$  formed in the pores of the silica matrix can be explained by the strong influence of the confined spaces on the crystallization process [28]. It is known that crystallization in mesopores can lead to the formation of crystals with deformed crystal lattices that are not observed in the bulk, even leading to new crystalline phases. Crystallization in porous media can affect a number of factors, including the nucleation rate, melting and solidification temperatures, and the polymorphism, size and morphology of the formed crystals. These structural changes may be due to both kinetic and thermodynamic reasons, where it is important to note that for a given volume, the geometry of the confining medium and the interfacial energy between crystals and the confining medium will ultimately determine the effect on crystallization. The chemical composition of the pore surface, undoubtedly, plays a role in the choice of polymorphic

form during crystallization from solution. A number of kinetic effects may also contribute to confined-space polymorphism. Reduced diffusion rates within small pores can result in a slow conversion between polymorphs and thus the stabilization of metastable phases [28].

### 3.3. Preparation—Properties Relation

The preparation of optical aerogel composites in this study is based on a two-step sol-gel process. In the first stage, we observe the formation of an inorganic silica aerogel matrix with a selected degree of hydrophobicity. Here, the aerogel matrix properties (hydrophobicity and pore architecture) can be tuned in order to obtain a suitable carrier for optically active species [2–4].

The next step is matrix functionalization. The matrix is soaked in a solution of an appropriate concentration of  $\text{Ln}(\text{NO}_3)_3$  ( $\text{Ln} = \text{Eu}, \text{Tb}$ ) in ethanol, followed by the addition of an ethanolic solution of 1,10-phenanthroline. After that, the granules are washed thoroughly with ethanol and dried at subcritical conditions; here, the efficacy of the drying procedure is checked by the very low thermal conductivity of the samples.

Our X-ray diffraction studies, quantum yield measurements and spectral intensity ratios demonstrate that the  $\text{Tb}^{3+}$ – $\text{Eu}^{3+}$  distance in the pores is very close (10 nm or less), resulting from the sol homogenization during the sol-gel process. There are indications of structural changes and  $[\text{Eu}, \text{Tb}(\text{phen})_2](\text{NO}_3)_3$  nanophase formation during the functionalization of the doped-aerogel porous matrix with 1,10-phenanthroline, proven by color coordinates and luminescence spectra analysis.

A comparison between aerogel composites and sol-gel composites shows some differences [29,30]. The high porosity of the aerogel-like materials allows an increased level of doping to be achievable, compared to other sol-gel samples. The hydrophobization of the silicate matrix also increases the thermal stability of aerogel composites and lowers their thermal conductivity [3]. Compared to single-doped composites, here, the doubly doped specimens have a different excitation spectrum and show small spectral differences due to physicochemical interaction in the aerogel pores.

## 4. Conclusions

An effective two-step sol-gel approach for the preparation of aerogel-like powders, binary-doped with  $[\text{Tb}(\text{phen})_2](\text{NO}_3)_3$  and  $[\text{Eu}(\text{phen})_2](\text{NO}_3)_3$  nanocrystals, is demonstrated. The as-prepared hydrophobic nanocomposites have a density of about  $0.2 \text{ g/cm}^{-3}$  and a thermal conductivity of about  $0.05 \text{ W/m.K}$ , dominated by the hydrophobicity and porosity of the aerogels. Luminescence, excitation spectra and quantum yield determination strongly suggest an effective energy transfer from the 1,10-phenanthroline molecule to the  $\text{Eu}^{3+}$  ion, resulting in a quantum yield of about 30% of the red europium f-f emission. Moreover, an energy transfer from the  $\text{Tb}^{3+}$  to the  $\text{Eu}^{3+}$  ion, leading to a suppression of green terbium f-f luminescence, is observed. An indication of a lowering of the site symmetry around  $\text{Eu}^{3+}$  ions, or the increased polarizability of the 1,10-phenanthroline ligand in the presence of Tb co-doping, is evident. There is also evidence for structural polymorphism in the binary composites, proven by X-ray diffraction and luminescence spectra analysis.

## 5. Materials and Methods

### 5.1. Sol-Gel Preparation

The following chemicals were used for the syntheses of the composite materials: absolute ethanol 99.6% (abs EtOH) (Merck, Darmstadt, Germany), 65% nitric acid (Fluka, Charlotte, North Carolina, US), europium (III) oxide 99.9% ( $\text{Eu}_2\text{O}_3$ ) (Merck, Darmstadt, Germany), terbium (III, IV) oxide 99.9% ( $\text{Tb}_4\text{O}_7$ ) (Merck, Darmstadt, Germany) and anhydrous 1,10-phenanthroline (Merck, Darmstadt, Germany) were used without further purification.

Non-doped aerogel-like samples without hydrophobization (GR0) were prepared using a standard procedure for sol-gel oxide powders, given in [4]. The starting reagent was TEOS, followed by  $\text{H}_2\text{O}$  addition, acid hydrolysis catalysis and basic gelation catalysis. The

ratio  $n_{\text{TEOS}}/n_{\text{H}_2\text{O}}$  was 1:1, while the acid and basic catalyst added were  $n_{\text{CH}_3\text{COOH}}/n_{\text{TEOS}} = 1.17$  and  $n_{\text{NH}_3}/n_{\text{TEOS}} = 0.04$ , respectively. The drying conditions applied were: room temperature and a pressure of 100 mbar.

Aerogel-like granules with a given degree of hydrophobicity  $\alpha = 1.1$  were synthesized through hydrolysis, solvent exchange, hydrophobization and drying using Tetraethyl orthosilicate (TEOS). Such aerogel powders have a bulk density of  $0.2 \text{ g/cm}^3$ , a specific surface area of  $870 \text{ m}^2/\text{g}$  and a mean pore diameter of 7 nm. Trimethyl chlorosilane (TMCS) was used as a hydrophobization agent. The degree of hydrophobicity,  $\alpha$ , is defined as the ratio between the moles of TMCS and TEOS. More details about the subcritical process used here can be found in [4].

Solutions of  $\text{Eu}(\text{NO}_3)_3$  and  $\text{Tb}(\text{NO}_3)_3$  were prepared by dissolving appropriate amounts of  $\text{Eu}_2\text{O}_3$  or  $\text{Tb}_4\text{O}_7$  in concentrated nitric acid. After the oxides dissolved, the solutions were heated to evaporate the leftover water, and nitric acid and transparent crystals were formed. The prepared salts were dissolved in absolute EtOH to obtain solutions with a concentration of 60 mM.

For the preparation of the aerogel-like composites, a two-step colloidal route was used, starting with hydrophobic silica micropowders, as described above. In the first step, hydrophobic  $\text{SiO}_2$  granules were soaked in  $\text{Eu}(\text{NO}_3)_3$ ,  $\text{Tb}(\text{NO}_3)_3$  or a mixture of both. The suspension was stirred for an hour to allow the solution to fill the pores of the gel. The molar ratio of  $\text{Ln}/\text{SiO}_2$  ( $\text{Ln} = \text{Eu}, \text{Tb}$ ) was fixed here at 0.01. In this way, both single functionalized composites ( $\text{SiO}_2:0.01[\text{Tb}(\text{phen})_2](\text{NO}_3)_3$  and  $\text{SiO}_2:0.01[\text{Eu}(\text{phen})_2](\text{NO}_3)_3$ ) and binary-doped composites ( $\text{SiO}_2:[\text{Eu}_x\text{Tb}_{1-x}(\text{phen})_2](\text{NO}_3)_3$ ) were obtained. For the preparation of binary-doped composites, an ethanol solution containing  $\text{Eu}^{3+}$  and  $\text{Tb}^{3+}$  nitrates was used. Afterwards, an excess solution of 1,10-phenanthroline (0.11 M in ethanol) was added, and the suspension was stirred for an additional hour. Then, the granules were filtered and washed thoroughly with ethanol, in order to remove the unreacted phen.

All samples were dried in an NÜVE vacuum oven at room temperature at a constant pressure of 100 mbar.

### 5.2. Optical Measurements

UV/Vis/NIR powder reflectance spectra were measured on an Agilent (Santa Clara, CA, USA) Cary 5000 spectrophotometer with a “Praying mantis” sample holder, using Spectralon<sup>®</sup> as a reference white standard between 200 nm and 2500 nm. The Kubelka–Munk function  $F(R)$  was calculated from the diffuse reflectance of all samples. As a standard for all diffuse reflection measurements,  $\text{Ho}_2\text{O}_3$  powder was used, and all peaks and relative intensities of the Ho(III) f-f transitions at 300–2000 nm were in agreement with spectral data published in [31].

The luminescence spectra of the powders were recorded on a PE (Shelton, CT, USA) FL 8500 fluorimeter equipped with an integrating sphere (N4201017) for absolute quantum yield (QY) measurements. The samples were placed in a quartz cell for the QY measurements. The absolute QY was obtained using the calculation method of Suzuki et al. [32]. The error of the QY determination here was about 5%.

Emission and excitation spectra were recorded using a variable-angle solid sample holder (N4201014) equipped with a precision cell for powder samples (N4201032). The calculation of  $x$  and  $y$  values was performed using a home-made program able to read the raw data file as it comes out from the instrument, based on the procedure published in [16]. The data points were validated through the OSRAM Sylvanya Color Calculator program. All the diffuse reflectance, excitation and emission spectra were quantified using Gaussian deconvolution.

### 5.3. X-ray Diffraction and Thermal Properties

The structure and microstructure of the samples were characterized by X-ray diffraction with Cu-K $\alpha$  radiation (Panalytical (Almelo, Netherlands) Empyrean 3 diffractometer). The mean crystallite sizes were calculated using Scherrer’s equation for the most

intense peak of  $[\text{Ln}(\text{phen})_2](\text{NO}_3)_3$ . The error of the lattice constant determination was about 0.005 Å. A qualitative phase analysis was performed on the following structures:  $[\text{Tb}(\text{phen})_2](\text{NO}_3)_3$ ,  $[\text{Eu}(\text{phen})_2](\text{NO}_3)_3$ , 1,10-phenanthroline,  $\text{Tb}(\text{NO}_3)_3$ , and  $\text{Eu}(\text{NO}_3)_3$ .

The thermal conductivities were measured on a C-Therm (C-Therm Technologies Ltd., Fredericton, NB, Canada) MTPS (Modified Transient Plane Source) TCi Thermal Conductivity Analyzer equipped with a powder and liquid sample holder. The error of the thermal conductivity determination of the gel powders was about 0.0002 W/m.K. At these conditions, the thermal properties of hydrophobic Cabot Lumira aerogel granules,  $\lambda = 0.0025$  W/m.K and  $e = 29.8$  W.s<sup>1/2</sup>/m<sup>2</sup>.K at 15.6 °C, were obtained as an external reference.

#### 5.4. Color Coordinates

Converting spectra to RGB (Red, Green, Blue) coordinates is a relatively common procedure in optical spectroscopy and analysis. The conversion allows for the visualization of fluorescence data in a color format, which is easily interpretable by the human eye. The acquired spectra were normalized and converted to XYZ coordinates by multiplying the spectral data by the respective color-matching curves [33]. The XYZ color coordinates were transferred to RGB (Red, Green, Blue) using the standard matrix conversion, with a reference white point of  $E = (0.333, 0.333, 0.333)$ , an sRGB color space, and Gamma correction (1.0) [34]. The values obtained in this procedure were compared with those obtained from free programs and websites, and full agreement was found.

**Author Contributions:** Conceptualization, S.G. and T.S.; methodology, S.G. and V.P.; software, V.P.; validation, V.P.; investigation, D.S., N.D., V.P., T.S. and S.G.; resources, T.S.; data curation, V.P.; writing—original draft preparation, D.S., N.D., T.S. and S.G.; writing—review and editing, S.G., T.S., D.S. and N.D.; visualization, D.S.; supervision, S.G.; project administration, T.S. All authors have read and agreed to the published version of the manuscript.

**Funding:** This research received no external funding.

**Informed Consent Statement:** Not applicable.

**Data Availability Statement:** The data presented in this study are openly available in article.

**Acknowledgments:** Thanks are due to the European Union-NextGenerationEU through the National Recovery and Resilience Plan of the Republic of Bulgaria, project No BG-RRP-2.004-0008. The authors are grateful to G. Avdeev for experimental help. SNIRD at STP is acknowledged for the technical support.

**Conflicts of Interest:** The authors declare no conflicts of interest.

## References

1. Aegerter, M.A.; Leventis, N.; Koebel, M.M. *Aerogels Handbook*; Springer: New York, NY, USA, 2011.
2. Gutzov, S.; Danchova, N.; Kirilova, R.; Petrov, V.; Yordanova, S. Preparation and Luminescence of Silica Aerogel Composites Containing an Europium (III) Phenanthroline Nitrate Complex. *J. Lumin.* **2017**, *193*, 108–112. [[CrossRef](#)]
3. Gutzov, S.; Shandurkov, D.; Danchova, N.; Petrov, V.; Spassov, T. Hybrid Composites Based on Aerogels: Preparation, Structure and Tunable Luminescence. *J. Lumin.* **2022**, *251*, 119171. [[CrossRef](#)]
4. Shandurkov, D.; Ignatov, P.; Spassova, I.; Gutzov, S. Spectral and Texture Properties of Hydrophobic Aerogel Powders Obtained from Room Temperature Drying. *Molecules* **2021**, *26*, 1796. [[CrossRef](#)]
5. Aguado, R.J.; Gomes, B.O.; Durães, L.; Valente, A.J.M. Luminescent Papers with Asymmetric Complexes of Eu(III) and Tb(III) in Polymeric Matrices and Suggested Combinations for Color Tuning. *Molecules* **2023**, *28*, 6164. [[CrossRef](#)]
6. Hull, R.R.M.; Osgood, J.; Paris, J.; Warlimont, H. *Spectroscopic Properties of Rare Earths in Optical Materials*; Springer: Berlin/Heidelberg, Germany, 2014; ISBN 3540238867.
7. Koseva, I.; Tzvetkova, P.; Ivanov, P.; Yordanova, A.; Nikolova, V. Terbium and Europium Co-Doped NaAlSiO<sub>4</sub> Nano Glass-Ceramics for LED Application. *Optik* **2017**, *137*, 45–50. [[CrossRef](#)]
8. Koseva, I.; Tzvetkov, P.; Ivanov, P.; Yordanova, A.; Nikolov, V. Some Investigations on Tb<sup>3+</sup> and Eu<sup>3+</sup> Doped Na<sub>2</sub>SiO<sub>3</sub> as a Material for LED Application. *Optik* **2018**, *168*, 376–383. [[CrossRef](#)]
9. Pawlik, N.; Szpikowska-Sroka, B.; Goryczka, T.; Pisarska, J.; Pisarski, W.A. Structural and Photoluminescence Investigations of Tb<sup>3+</sup>/Eu<sup>3+</sup> Co-Doped Silicate Sol-Gel Glass-Ceramics Containing CaF<sub>2</sub>, Nanocrystals. *Materials* **2021**, *14*, 754. [[CrossRef](#)]

10. Han, S.; Tao, Y.; Du, Y.; Yan, S.; Chen, Y.; Chen, D. Luminescence Behavior of GdVO<sub>4</sub>: Tb Nanocrystals in Silica Glass-Ceramics. *Crystals* **2020**, *10*, 396. [[CrossRef](#)]
11. Halubek-Gluchowska, K. Upconversion Luminescence of Silica–Calcium Nanoparticles Co-Doped with Tm<sup>3+</sup> and Yb<sup>3+</sup> Ions. *Materials* **2021**, *14*, 937. [[CrossRef](#)]
12. Kameneva, S.V.; Yorov, K.E.; Kamilov, R.K.; Kottsov, S.Y.; Teplonogova, M.A.; Khamova, T.V.; Popkov, M.A.; Tronev, I.V.; Baranchikov, A.E.; Ivanov, V.K. Epoxide Synthesis of Binary Rare Earth Oxide Aerogels with High Molar Ratios (1:1) of Eu, Gd, and Yb. *J. Sol-Gel Sci. Technol.* **2023**, *107*, 586–597. [[CrossRef](#)]
13. Zhang, Y. *High-Entropy Materials: A Brief Introduction*; Springer: Singapore, 2019; ISBN 978-981-13-8526-1.
14. Workman, J.; Weyer, L. *Practical Guide to Interpretive Near-Infrared Spectroscopy*; CRC Press: Boca Raton, FL, USA; Taylor & Francis Group: Abingdon, UK, 2008; ISBN 13: 978-1-57444-784-2.
15. Mirochnik, A.G.; Bukvetskii, B.V.; Zhikhareva, P.A.; Karasev, V.E. Crystal Structure and Luminescence of the [Eu(Phen)<sub>2</sub>(NO<sub>3</sub>)<sub>3</sub>] Complex. The Role of the Ion-Coactivator. *Russ. J. Coord. Chem.* **2001**, *27*, 443–448. [[CrossRef](#)]
16. Xie, T.; He, Y.-L.; Hu, Z.-J. Theoretical Study on Thermal Conductivities of Silica Aerogel Composite Insulating Material. *Int. J. Heat Mass Transf.* **2013**, *58*, 540–552. [[CrossRef](#)]
17. Wei, D.-Y.; Lin, J.-L.; Zheng, Y.-Q. Note: The Crystal Structure of Tris(Nitrato-O,O')Bis(1,10-Phenanthroline-N,N')Terbium(III). *J. Coord. Chem.* **2002**, *55*, 1259–1262. [[CrossRef](#)]
18. Zahariev, T.; Shandurkov, D.; Gutzov, S.; Trendafilova, N.; Enseling, D.; Jüstel, T.; Georgieva, I. Phenanthroline Chromophore as Efficient Antenna for Tb<sup>3+</sup> Green Luminescence: A Theoretical Study. *Dye. Pigment.* **2020**, *185*, 108890. [[CrossRef](#)]
19. Binnemans, K. Interpretation of Europium(III) Spectra. *Coord. Chem. Rev.* **2015**, *295*, 1–45. [[CrossRef](#)]
20. Blasse, G.; Grabmaier, B.C. *Luminescent Materials*; Springer: Berlin/Heidelberg, Germany, 1994.
21. Fujishiro, F.; Murakami, M.; Hashimoto, T.; Takahashi, M. Orange Luminescence of Eu<sup>3+</sup> Doped CuLaO<sub>2</sub> Delafossite Oxide. *J. Ceram. Soc. Japan* **2010**, *118*, 1217–1220. [[CrossRef](#)]
22. Gomez-Romero, P.; Sanchez, C. *Functional Hybrid Materials*; Wiley-VCH: Hoboken, NJ, USA, 2003; ISBN 9781787284395.
23. Dieke, G.H.; Crosswhite, H.M.; Crosswhite, H. *Spectra and Energy Levels of Rare Earth Ions in Crystals*; Interscience Publishers: New York, NY, USA, 1968; ISBN 0470213906.
24. Singh, S.; Singh, D. Synthesis and Spectroscopic Investigations of Trivalent Europium-Doped M<sub>2</sub>SiO<sub>5</sub> (M = Y and Gd) Nanophosphor for Display Applications. *J. Mater. Sci. Mater. Electron.* **2020**, *31*, 5165–5175. [[CrossRef](#)]
25. Boruc, Z.; Fetlinski, B.; Kaczkan, M.; Turczynski, S.; Pawlak, D.A.; Malinowski, M. Temperature and Concentration Quenching of Tb<sup>3+</sup> Emissions in Y<sub>4</sub>Al<sub>2</sub>O<sub>9</sub> Crystals. *J. Alloys Compd.* **2012**, *532*, 92–97. [[CrossRef](#)]
26. Culubrk, S.; Lojpur, V.; Antic, Z.; Drami, M.D. Structural and Optical Properties of Europium Doped Y<sub>2</sub>O<sub>3</sub> Nanoparticles Prepared by Self-Propagation Room Temperature Reaction Method. *J. Res. Phys.* **2013**, *37*, 39–45. [[CrossRef](#)]
27. Shandurkov, D.; Danchova, N.; Spassov, T.; Petrov, V.; Tsekov, R.; Gutzov, S. Silica Gels Doped with Gold Nanoparticles: Preparation, Structure and Optical Properties. *Gels* **2023**, *9*, 663. [[CrossRef](#)]
28. Meldrum, F.C.; O'Shaughnessy, C. Crystallization in Confinement. *Adv. Mater.* **2020**, *32*, 2001068. [[CrossRef](#)] [[PubMed](#)]
29. Brinker, J.C.; Scherer, G.W. *The Physics and Chemistry of Sol-Gel Processing*; Academic Press, INC: London, UK, 1990.
30. Schmidt, H. *Sol-Gel Production*; Trans Tech Publications Ltd.: Uetikon-Zürich, Switzerland, 1998.
31. Yadav, R.; Sardar, S.; Singh, M.; Mukherjee, R.K.; Anju, Singh, S.; Kushwaha, P.; Singh, S.P. Preparation of Holmium Oxide Solution as a Wavelength Calibration Standard for UV–Visible Spectrophotometer. *Mapan J. Metrol. Soc. India* **2021**, *37*, 579–584.
32. Suzuki, K.; Kobayashi, A.; Kaneko, S.; Takehira, K.; Yoshihara, T.; Ishida, H.; Shiina, Y.; Oishi, S.; Tobita, S. Reevaluation of Absolute Luminescence Quantum Yields of Standard Solutions Using a Spectrometer with an Integrating Sphere and a Back-Thinned CCD Detector. *Phys. Chem. Chem. Phys.* **2009**, *11*, 9850–9860. [[CrossRef](#)] [[PubMed](#)]
33. Wyman, C.; Sloan, P.-P.; Shirley, P. Simple Analytic Approximations to the CIE XYZ Color Matching Functions. *J. Comput. Graph. Tech.* **2013**, *2*, 11.
34. Pharr, M.; Jakob, W.; Humphreys, G. *Physically Based Rendering: From Theory to Implementation*; The MIT Press: Cambridge, MA, USA, 2023; ISBN 978-0262048026.

**Disclaimer/Publisher's Note:** The statements, opinions and data contained in all publications are solely those of the individual author(s) and contributor(s) and not of MDPI and/or the editor(s). MDPI and/or the editor(s) disclaim responsibility for any injury to people or property resulting from any ideas, methods, instructions or products referred to in the content.